ACS OMEGA

http://pubs.acs.org/journal/acsodf

Article

Microwave-Epoxide-Assisted Hydrothermal Synthesis of the CuO/ZnO Heterojunction: a Highly Versatile Route to Develop H_2S Gas Sensors

Digambar Y. Nadargi, Mohaseen S. Tamboli, Santosh S. Patil, Ramesh B. Dateer, Imtiaz S. Mulla, Hyosung Choi,* and Sharad S. Suryavanshi*

Cite This: *ACS Omega* 2020, 5, 8587−8595

Read Online

ACCESS | Metrics & More | Article Recommendations | Supporting Information

ABSTRACT: A robust synthesis approach to develop CuO/ZnO nanocomposites using microwave-epoxide-assisted hydrothermal synthesis and their proficiency toward H_2S gas-sensing application are reported. The low-cost metal salts (Cu and Zn) as precursors in aqueous media and epoxide (propylene oxide) as a proton scavenger/gelation agent are used for the formation of mixed metal hydroxides. The obtained sol was treated using the microwave hydrothermal process to yield the high-surface area (34.71 m^2/g) CuO/ZnO nanocomposite. The developed nanocomposites (1.25−10 mol % Cu doping) showcase hexagonal ZnO and monoclinic CuO structures, with an average crystallite size in the range of 18−29 nm wrt Cu doping in the ZnO matrix. The optimized nanocomposite (2.5 mol % Cu doping) showed a lowest crystallite size of 21.64 nm, which reduced further to 18.06 nm upon graphene oxide addition. Morphological analyses (scanning electron microscopy and transmission electron microscopy) exhibited rounded grains along with copious channels typical for sol−gel-based materials . Elemental mapping displayed the good dispersion of Cu in the ZnO matrix. When these materials are employed as a gas sensor, they demonstrated high sensitivity and selectivity toward H_2S gas in comparison with the reducing gases and volatile organic compounds under investigation. The systematic doping of Cu in the ZnO matrix exhibited an improved response from 76.66 to 94.28%, with reduction in operating temperature from 300 to 250 °C. The 2.5 mol % doped Cu in ZnO was found to impart a response of 23 s for 25 ppm of H_2S. Gas-sensing properties are described using an interplay of epoxide-assisted sol−gel chemistry and structural and morphological properties of the developed material.

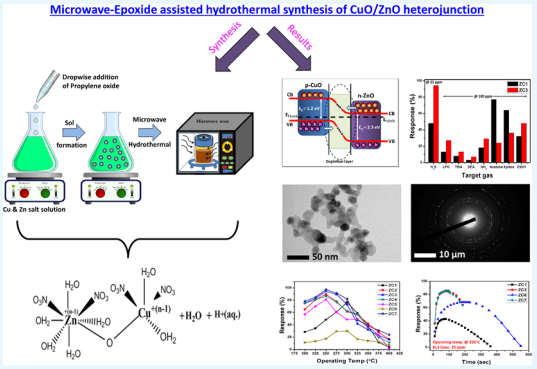

INTRODUCTION

Over the past two decades, metal oxide semiconductor-based gas sensors have attracted great attention among researchers because of their robustness, low production cost, high sensitivity, and the ability to detect various gases.[1−6] Despite two main types of semiconducting metal oxide-based sensors, such as n-type (electrons as majority charge carriers) and p-type (holes as majority charge carriers), the construction of heterojunction (p−n) sensors has become an efficient approach to improve the sensing performance. When two such dissimilar semiconductors are brought together, the Fermi level of individual semiconductors reside at the same energy level upon electrical contact. This in turn results in charge transfer and, thereby, the formation of a depletion layer. This is the basis of unique synergistic effects to the substantial enhancement in the gas response compared with their single component system.[7,8]

In the present work, efforts were made to develop the CuO/ZnO heterojunction using epoxide-assisted sol−gel chemistry in combination with the microwave hydrothermal process. In the state-of-the-art, despite significant investigations on CuO/ZnO in recent years,[9−15] this is the first ever report that disseminates the results on the epoxide [propylene oxide (PO)]-assisted sol−gel process of the CuO/ZnO heterojunction via a microwave hydrothermal route for H_2S gas-sensing proficiency. This robust synthesis approach utilizes simple metal salts in aqueous solution and PO as a gelation agent.[16] Scheme 1 shows a schematic illustrating the formation of CuO/ZnO nanocomposites from the respective metal salts [zinc nitrate hexahydrate ($Zn(NO_3)_2{\cdot}6H_2O$), copper nitrate trihydrate ($Cu(NO_3)_2{\cdot}3H_2O$), and PO (C_3H_6O)]. Assuming a strenuous reaction mechanism for CuO/ZnO sol, for example, a nitrate-aqua metal cation (present case), the epoxide ring is attacked by a nucleophile, namely, a "free" uncoordinated

Received: December 29, 2019
Accepted: February 27, 2020
Published: April 10, 2020

Scheme 1. Schematic Showing the PO-Assisted Sol−Gel Reaction Mechanism of the CuO/ZnO Nanocomposite

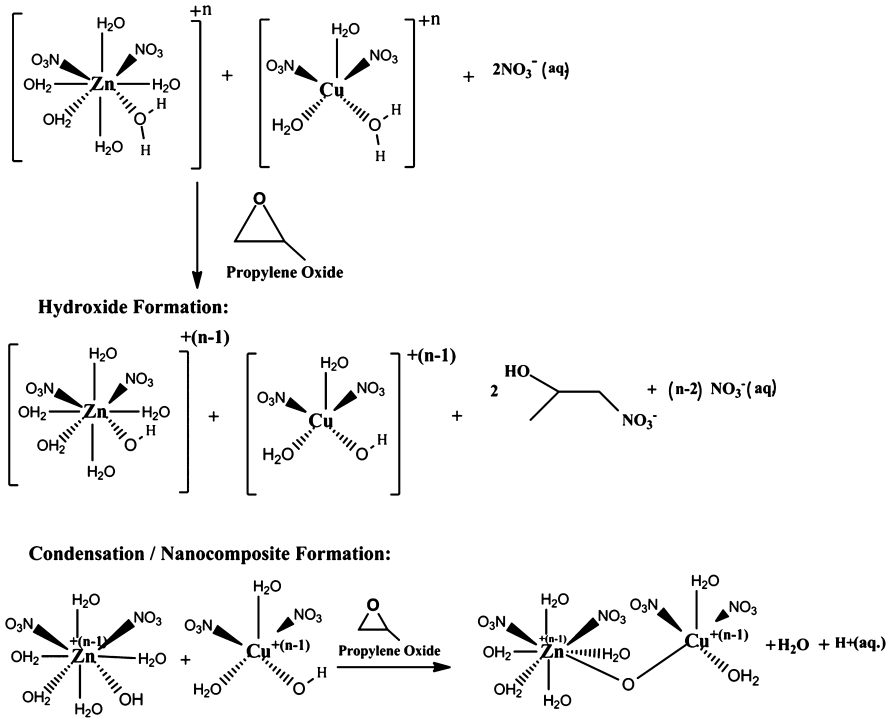

corresponding anion of the metal salt NO_3^-. As the ring opens, a proton from a water ligand molecule is abstracted, thereby yielding the mixture of nitrate-aquametal hydroxides. The formation of metal−oxygen−metal bonds (condensation reaction) can be simply viewed as a ligand-substitution reaction. As water is an easily detachable group, the kinetics of the reaction are primarily determined by the pH and nature of the attacking nucleophile.

Different types of epoxides such as PO (C_3H_6O), trimethylene oxide (TMO, C_3H_6O), and dimethyloxetane (DMO, $C_5H_{10}O$) can be used for the aforementioned reaction chemistry. However, the rate of the proton scavenging reaction strongly depends on the type of epoxide used. Gash et al. reported the gelation times to increase with the epoxide used in the order PO < TMO < DMO.[17] Therefore, in the present work, PO is preferred to adopt for the sol−gel process to develop CuO/ZnO nanocomposites.

Speaking about an adoption of the microwave hydrothermal route, it refers to the utilization of microwave radiation as a heat source for the nanocomposite synthesis. In contrast to the conventional hydrothermal process where heat transfer occurs via convection, microwaves directly couple to the reactant species, thus eliminating the traditional/long heating reaction times. Also, as the microwaves couple well to electric dipoles, the high polarity of H_2O in an aqueous solution for hydrothermal synthesis is ideally suited for microwave heat exposure.[18,19]

The present work demonstrated, the adoption of the microwave hydrothermal process and use of epoxide-assisted colloidal chemistry, which led to promising results in the development of CuO/ZnO heterojunctions as a highly versatile H_2S gas sensor material.

The adopted route (epoxide assisted sol−gel process) offers a number of advantages such as the route utilizes simple metal salts in aqueous solution, typically metal nitrates/chlorides/halides, thus eliminating the need for expensive organometallic precursors in some typical cases with the use of an alcohol solvent medium. With an eye on large scale production, the absence of surfactants/capping agents and alcohol solvents, the use of simple salt precursors, and, perhaps most importantly, the rapid processing times are unique features of this technique. Prior to microwave hydrothermal treatment, even without heating the reagents, the reaction moieties are formed almost instantaneously, depending on the amount of PO utilized. The method is, in general, very well-suited for the synthesis of a variety of complex mixed metal oxide materials. Last but not the least, the process allows improved control over the morphology of the resulting nanocomposite/mixed metal oxide. The detailed comparison on the state-of-the-art articles with the present results is made in the supplementary section (Table S1).

RESULTS AND DISCUSSION

The developed nanocomposites showcase hexagonal ZnO and monoclinic CuO structures, matching with the patterns of JCPDS cards 36-1451 and 89-5899, respectively (Figure 1).

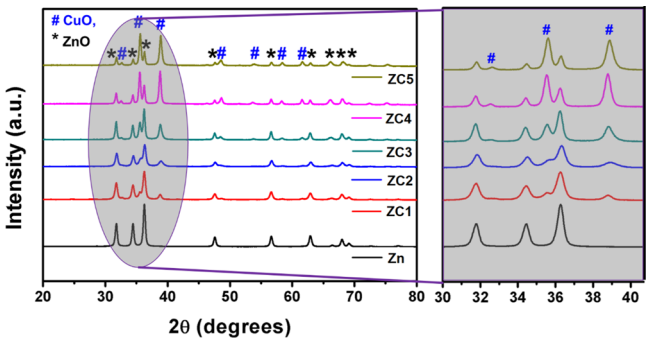

Figure 1. X-ray diffraction (XRD) pattern of CuO/ZnO nanocomposites synthesized at different doping levels.

https://dx.doi.org/10.1021/acsomega.9b04475
ACS Omega 2020, 5, 8587−8595

The miller indices of the developed nanocomposite were observed as (1 0 0), (0 0 2), ($\bar{1}$ 1 1), (1 0 1), (1 1 1), (1 0 2), ($\bar{2}$ 0 2), (0 2 1), ($\bar{1}$ 1 3), (1 0 3), (2 0 0), (2 2 0), and (2 0 1) for 31, 34, 35, 36, 38, 47, 48, 56, 61, 62, 66, 68, and 69°, respectively, with a bar indicating the negative direction of the plane. The well-resolved sharp peaks of ZnO (1 0 1) and CuO (1 1 1), ($\bar{1}$ 1 1) signifies the highly crystalline formation of the CuO/ZnO heterojunction.[20] With an increase in the doping level of Cu in the ZnO matrix, the peak intensity of the CuO plane (1 1 1) was observed to increase. No diffraction peak corresponding to any other crystalline phase of Cu_2O_3 implies the proper dispersion of Cu into the ZnO lattice. The average crystallite size using the Scherrer equation (eq 1) was obtained in the range of 18−29 nm, according to Cu doping in the host matrix.

$$D = K\lambda/\beta \cos\theta$$

1where K—Debye−Scherrer's constant, λ—wavelength of the radiation (Cu Kα_1 = 0.154 nm), β—full width half maximum, and θ—Bragg's angle.

The sample ZC2 shows the lowest crystallite size of 21.64 nm, which reduced further to 18.06 nm, upon graphene oxide (GO) addition (sample GO_ZC2). The reduced/lower crystallite size gives the hint of a potential candidate for gas-sensing application because of the fact that the smaller crystallite size offers a larger surface area [revalidated using Brunauer−Emmett−Teller (BET) in the later section]. Therefore, the probability of gas−solid interaction will be enhanced because of larger coverage of the gas molecules.[21] Table 1 below tabulates the average crystallite size (D_{XRD}) from XRD for all the developed samples.

Table 1. Average Crystallite Size (D_{XRD}) from XRD for all the Developed Samples

sample id	average crystallite size D_{XRD} (nm)
Zn	26.27
ZC1	21.71
ZC2	21.64
ZC3	28.06
ZC4	28.61
ZC5	29.85
GO_ZC2	18.06

The morphological analysis of pristine and optimized Cu-doped ZnO samples (Zn & ZC2) is highlighted in Figure 2. Field emission scanning electron microscopy (FE-SEM) images showcase the peculiar features of sol−gel derived nanomaterials.[16] The grain size of the sample obtained from FE-SEM micrographs is in the range of 34−63 nm. The rounded grains along with copious channels can be attributed to the formation of the three-dimensional web matrix of the metal oxide because of the epoxide-assisted gelation process. The three dimensional web matrix can be easily noticed in transmission electron microscopy (TEM) and high-resolution TEM (HRTEM) images of respective samples. Such empty spaces and channels allow effective diffusion of gas molecules for an improved gas-sensing response. Moreover, the HRTEM fringes and selected area electron diffraction (SAED) patterns with bright rings match with pristine and doped ZnO planes belonging to the hexagonal ZnO and monoclinic CuO structures, thus revalidating the results obtained from XRD analysis.

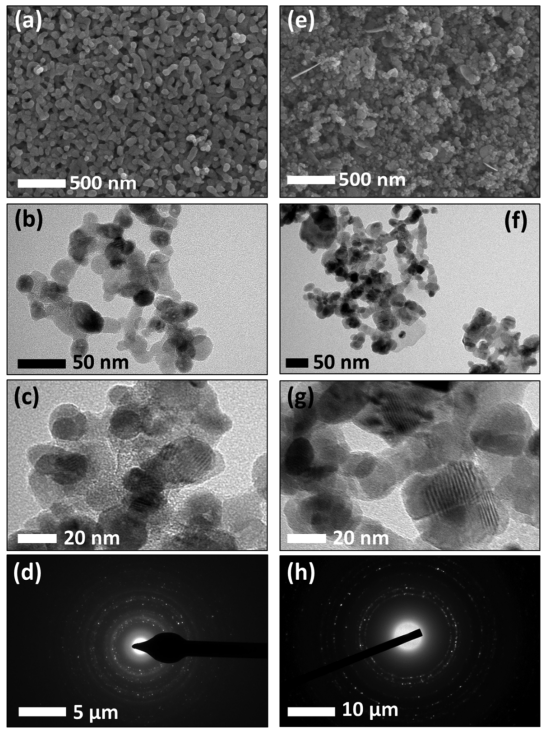

Figure 2. FE-SEM, TEM, HRTEM, and SAED pattern of CuO/ZnO nanocomposites [sample Zn: (a−d), and sample ZC2: (e−h)].

The energy dispersive X-ray (EDAX) analysis for sample Zn and GO_ZC2 shows the presence of Zn, Cu, and O elements according to atomic ratios taken in the initial precursors (Figure 3). The elemental distribution and EDAX analysis of the sample ZC2 are incorporated into the supplementary section, as Figures S4 and S5, respectively. The atomic ratios of the constitutive elements are highlighted in percentage within Figure 3. Its elemental mapping illustrates the uniform distribution of Cu in the ZnO matrix. The corresponding EDS spectrum (right side) provides the compositional elements wrt their counts.

From N_2 sorption studies (Figure 4), the developed nanocomposites showcase the characteristic behavior of a type-IV isotherm which is typical for mesopores, with a well-defined hysteresis loop of type H3 (indicating platelike particles forming slit-shaped pores) at $p/p_0 > 0.9$.[22] As hysteresis is usually associated with capillary condensation in mesoporous structures, the decrease in the adsorbed volume in samples Zn and ZC5 resulted in a lower surface area than ZC2 and GO_ZC2. With an addition of GO in the optimized Cu-doped ZnO sample (ZC2), it evolves with the highest surface area (34.71 m^2/g), which is anticipated for better gas response. The resulting higher surface-to-volume ratio in GO_ZC2 is due to addition of GO, which inhibits the growth the particles (seen in XRD as well). Table 2 highlights the mean pore radius, pore volume, and BET surface area of all developed samples.

Gas Response Analysis. To investigate and compare the gas-sensing performance of the developed CuO/ZnO nanocomposites, the respective sensors were tested for different reducing gases and volatile organic compounds (H_2S, LPG, trimethylamine, diethanolamine, ammonia, acetone, xylene, and ethanol). Among all the test gases, the CuO/ZnO nanocomposite (ZC2) displayed the best selectivity toward

https://dx.doi.org/10.1021/acsomega.9b04475
ACS Omega 2020, 5, 8587−8595

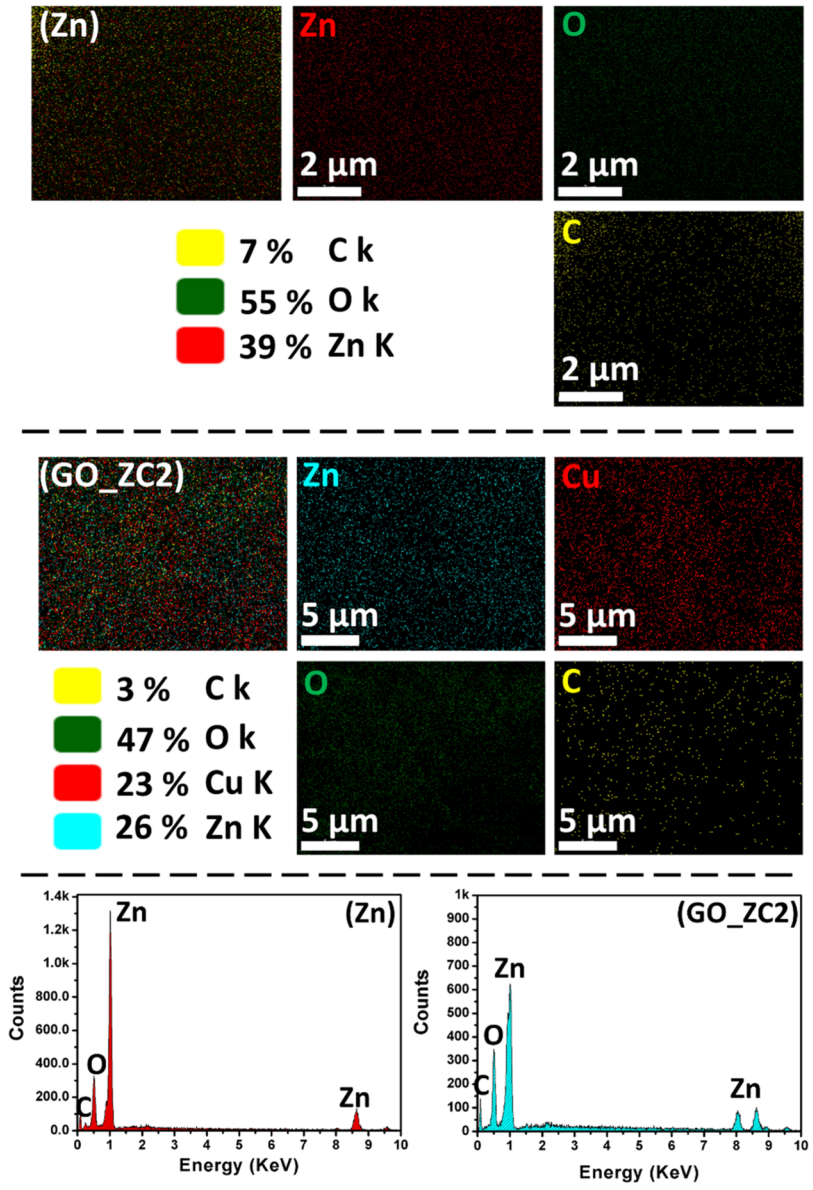

Figure 3. Elemental mapping along with the EDX spectra of the sample Zn and GO_ZC2.

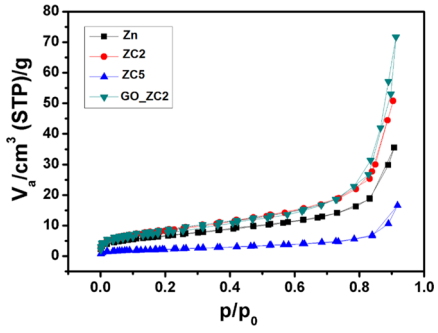

Figure 4. Nitrogen absorption−desorption isotherms of samples Zn, ZC2, ZC5, and GO_ZC2.

H_2S gas (Figure 5a) with remarkable 94% response at barely 25 ppm H_2S concentration at 250 °C operating temperature. Because of Cu doping in the ZnO matrix, the response shoot up twice of pristine's response (Zn, 48%). In contrast, none of the remaining test gases showed comparable response even at 100 ppm gas concentration. Therefore, by considering H_2S selectivity, further investigations were performed.

Figure 5b displays the optimal operating temperature (OOT onward) of the developed sensor material toward H_2S. The sensors (pristine and nanocomposites) displayed the hump, indicating (i) increase in gas response, (ii) realization of a certain maxima, and (iii) and further decrease with increasing

Table 2. Mean Pore Radius, Pore Volume, and BET Surface Area of the Developed CuO/ZnO Nanocomposites

sample id	mean pore diameter (nm)	pore volume (m^3/g) × 10^{-8}	surface area (m^2/g)
Zn	9.29	5.5	23.61
ZC1	10.20	7.9	30.47
ZC2	8.82	7.7	31.59
ZC3	10.92	5.0	18.39
ZC4	12.71	2.6	8.09
ZC5	11.62	2.1	7.36
GO_ZC2	14.56	1.1	34.71

https://dx.doi.org/10.1021/acsomega.9b04475
ACS Omega 2020, 5, 8587−8595

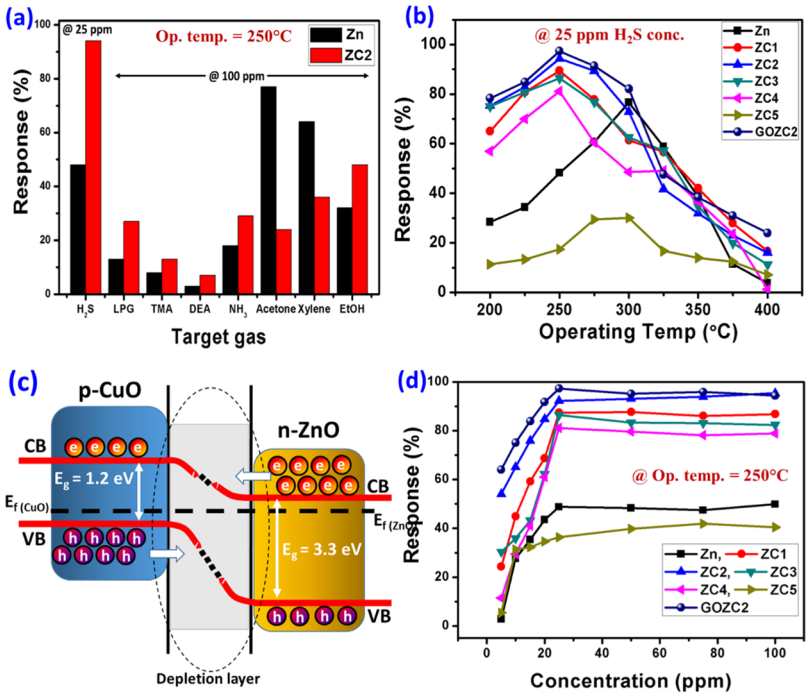

Figure 5. Gas sensing analyses [(a) selectivity, (b) optimum operating temperature, and (d) concentration response] and (c) formation of the p−n junction of the CuO/ZnO nanocomposite.

operating temperature. The nature is the result of adsorption and desorption of oxygen molecules from the sensor surface, which is extensively reported.[23,24] Initially, when the pristine ZnO (sample Zn) was exposed to air, oxygen molecules chemisorbed on the sensor surface and then capture the conduction band (CB) electrons to generate ionized oxygen species such as O_2^-, O^-, and O^{2-}, which results in an increase in the resistance of the ZnO sensor because of the formation of electron depletion layers. However upon adding H_2S gas, it reacts with these chemisorbed oxygen ions, and then releases the trapped electrons back to ZnO. As a result, the width of the depletion layer decreases and thus the resistance as well. The possible reactions are as follows[25]

$$O_2 + 2e^- \rightarrow 2O^- \quad (1)$$

$$H_2S + 3O^- \rightarrow H_2O + SO_2 + 3e^- \quad (2)$$

On the other hand, the introduction of CuO in the ZnO matrix (thus forming a p−n heterojunction) enhanced the sensing performance drastically. The improved sensing performance of the CuO/ZnO p−n heterojunction sensor compared to that of the pristine one can be attributed to the electronic and chemical sensitization effects transpired because of CuO incorporation. Talking about electronic sensitization, a typical p−n heterojunction is established between p-type CuO and n-type ZnO. Because the work function of Cu (4.53−5.10 eV) is higher than that of Zn (3.63−4.9 eV), the electrons in the ZnO CB transfer to CuO, while the holes transfer toward ZnO until the Fermi level (E_f) of the junction comes to equilibrium. This widens the depletion layer, and thus, energy band bending occurs at the interface of the CuO/ZnO p−n heterojunction, thereby improving the response (Figure 5c).

On the other hand, in the chemical sensitization effect (catalytic spillover effect), CuO plays an important role. It acts as a catalyst which facilitates the dissociation of oxygen molecules into O atoms.[26]

$$O_{2(gas)} \leftrightarrow 2O_{(ads)} \quad (3)$$

The generated O atoms get diffuse and spill over onto the ZnO surface. The diffused O atoms trap the electrons from CB of ZnO and creates adsorbed O^- ions on the sensor surface.

$$O_{(ads)} + e_{(\text{from ZnO})}^- \leftrightarrow O_{(ads)}^- \quad (4)$$

This phenomenon results in the increase in the number of chemisorbed oxygen species on the CuO/ZnO p−n heterojunction as compared to that on pristine ZnO. In this situation, a greater number of electrons will be extracted from ZnO, which eventually increases the depletion layers between the ZnO and CuO, resulting a wider depletion layer and band bending at the interface. This results in high potential barrier (qV) between the intergranular ZnO and CuO junction, which hinder the conduction of electrons, thus increasing the resistance of the sensor. After the exposure with H_2S gas, the chemisorbed oxygen ions (O^-) react with H_2S gas molecules and release the trapped electrons back to the CB of ZnO and CuO. This results in the lowering of the potential barrier height and decrease of the resistance of the CuO/ZnO p−n heterojunction. Hence, the chemical sensitization effect accelerates the sensing reaction with improved sensing performance. Moreover, CuO not only increases the sites for the oxygen molecule and target gas adsorption but also lowers the activation energy that is required for the gas-sensing reaction. Therefore, the response of the CuO/ZnO p−n heterojunction (sample ZC2) is much higher. Furthermore, it was reported that CuO can be reduced to Cu, with electrons being donated back to the heterojunction, upon exposing to reducing gases (H_2S). This also results into reduction of depletion layer width, thereby inducing a large resistance change in the heterojunction.

Another important aspect in the chemical sensitization is transformation of CuO to CuS upon an introduction of H_2S

https://dx.doi.org/10.1021/acsomega.9b04475
ACS Omega 2020, 5, 8587−8595

gas, through the sulphurization reaction.[27] The sulphurization reaction can be shown as follows[28]

$$CuO_{(s)} + H_2S_{(g)} \rightarrow CuS_{(s)} + H_2O_{(g)} \quad (5)$$

The work function of CuO is 3.61 eV, whereas CuS has in the range of 4.90−4.95 eV.[29−32] Because of the difference in the work function, electrons from CuO flow to CuS, establishing the potential barrier. When only the grain boundary regions are converted to CuS, the width of the potential barrier narrows down (at lower concentration of H_2S). Therefore, it changes the conductivity from semiconducting to metallic type leading to a high response toward H_2S.[33−39] The following Scheme 2, illustrates the energy band structure of the developed CuO/ZnO nanostructure, before and after H_2S gas sensing. CuO nanoparticles (p-type) which are the part of the ZnO matrix (n-type) forms a p−n junction (Scheme 2a). In origin, the junctioned sensor material show high conductivity (0.2 μA in air) compared to that of the pristine metal oxide/nonjunctioned sensor material (0.5 μA in air). During H_2S gas sensing, the H_2S removes the adsorbed oxygen species on ZnO and reacts with CuO to convert into metallic CuS (eq 5). This chemical conversion of CuO into metallic CuS led to increase the conductivity, thereby change in the energy band structure (Scheme 2b). During the recovery mode, on the application air purge, the sensor comes back to the initial chemical state as of the fresh CuO/ZnO junction, through the chemical revision of CuS to CuO (eq 6) by the reaction with oxygen in air. This way an ionized oxygen species adsorb back onto the ZnO again.

Scheme 2. Schematic Illustrating the Energy Band Structure of the Developed CuO/ZnO Nanostructure, before and after H_2S Gas Sensing

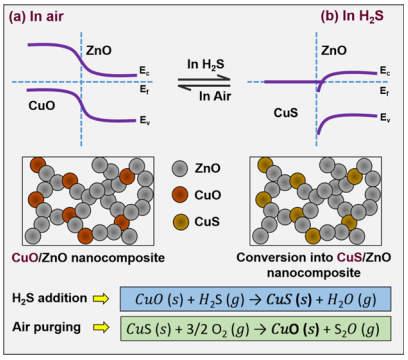

$$CuS_{(s)} + 3/2O_{2(g)} \rightarrow CuS_{(s)} + S_2O_{(g)} \quad (6)$$

Also, from BET, it has been validated that the CuO/ZnO sample with optimum Cu doping (sample ZC2) has a larger surface area. Therefore, it possesses more surface adsorption sites and better gas diffusion as compared with the pristine one, which facilitated an enhanced sensing performance.

Notably, considerable performance difference was observed between pristine and Cu-doped ZnO nanocomposites. Two targets in one bullet were achieved by proper doping of Cu in the ZnO matrix. Not only sensor response was improved (from 76.66 to 94.28%) but also the operating temperature reduced (from 300 to 250 °C). The optimized doping of Cu was found to be 2.5 mol % in the ZnO matrix (Sample ZC2), which showed proper phase formation (as seen in XRD signatures) and the highest surface area favoring the effective diffusion and acceleration of a target gas. Figure 5d shows the sensor response as a function of H_2S concentration. In the initial stage (upto 20 ppm), the sensitivity rapidly increased with a greater slope. With further increase in the H_2S concentration, the sensitivity increased more or less with saturation. Such a behavior is obvious because of the loss of surface active sites for the interaction with gas molecules.

Figure 6a highlights the transient response curve of pristine and doped ZnO samples (Zn, ZC2, ZC5, and GO_ZC2),

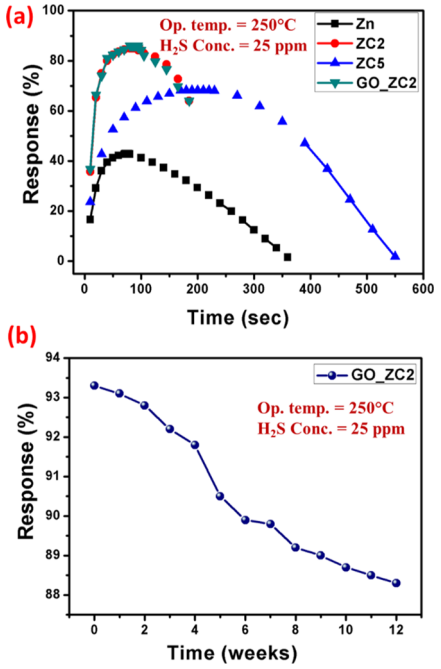

Figure 6. Gas sensing performance of the developed sensors, (a) transient response, and (b) stability over the period of 12 weeks.

where almost the U shape is obtained for best optimized samples, ZC2 and GO_ZC2. It directs the obtained sensing material as the best candidate for H_2S sensing, with quick response of 23 s for 25 ppm of H_2S. Finally, the optimized sample GO_ZC2 was tested for its stability over the period of 12 weeks (Figure 6b). It has been observed that the sample showed almost 95% of its initial sensitivity, confirming the suitability of the developed material for commercial applications as the H_2S sensor.

CONCLUSIONS

In conclusion, we have developed a simple synthesis strategy of fabricating a CuO/ZnO p−n heterojunction by a microwave-epoxide assisted sol−gel process for the first time and thereby its proficiency toward H_2S gas-sensing application. The versatile method utilizes inexpensive precursors (metal salts) in aqueous solution with PO as the gelation agent. Its inherent simplicity made it feasible to fabricate virtually any type of mixed-metal oxide nanocomposites with ease. The developed nanocomposites (CuO/ZnO) exhibited smaller crystallite size (18 nm) with a larger surface area (34.71 m^2/g), proving their proficiency toward gas−solid interactions. The rounded grains (usually seen in the sol−gel process) with the 3D network structure yielded copious channels for gas diffusion. Elemental mapping highlights the good dispersion of Cu in the ZnO matrix. Upon employing these nanocomposites as gas sensors,

https://dx.doi.org/10.1021/acsomega.9b04475
ACS Omega 2020, 5, 8587−8595

Scheme 3. Schematic Illustrating (a) the Complete Synthesis Process, and (b) Various Samples Prepared in This Study

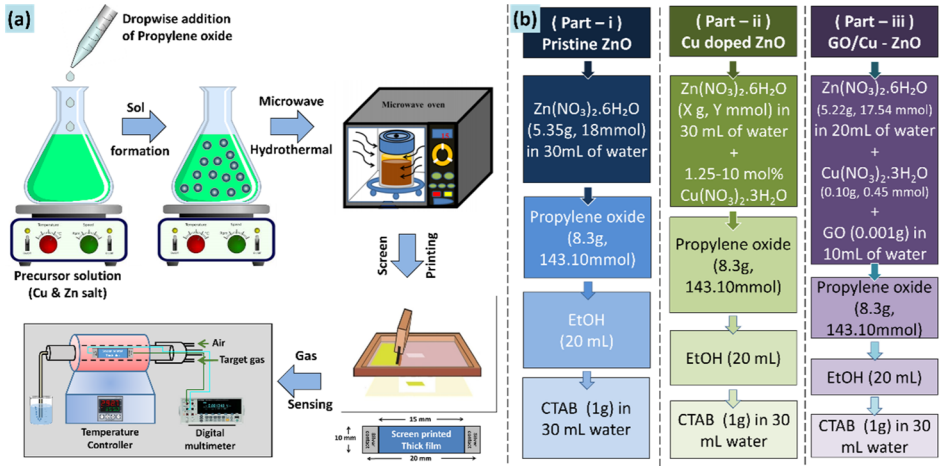

they demonstrated high sensitivity and selectivity to H_2S gas. The sensor response was improved from 76.66 to 94.28%, with reduction in the operating temperature from 300 to 250 °C. The 2.5 mol % doping of Cu in ZnO was found to impart a quick response of 23 s for 25 ppm of H_2S. GO loading in the abovementioned optimized Cu-doped ZnO resulted in almost 95% retention of its initial sensitivity, even after 12 weeks of shelf life. The reported approach of fabricating the gas sensor is easily reproducible and cost effective, thus offering great promise for future industrial application of H_2S gas sensors.

EXPERIMENTAL SECTION

The chemicals used in a typical synthesis were zinc nitrate hexahydrate ($Zn(NO_3)_2{\cdot}6H_2O$), copper nitrate trihydrate ($Cu(NO_3)_2{\cdot}3H_2O$), GO, PO, and hexadecytrymethylammoniumbromide (CTAB). All reactants were reagent grade quality obtained from Sigma-Aldrich and were used as received. Double distilled water (DW) was used for the complete synthesis process. Scheme 3 below contains a simplified schematic illustrating the complete experimental process (Scheme 3a), along with the preparation of the various sample groups discussed in this work (Scheme 3b).

In part-i, pristine ZnO was prepared by dissolving $Zn(NO_3)_2{\cdot}6H_2O$ (5.35 g, 18 mmol) in 30 mL of DW, followed by the slow and dropwise addition of PO (8.3 g, 143.10 mmol). This mode of addition of PO is preferred because rapid addition results in significant heat evolution given the exothermic nature of the reaction. Dropwise addition of the given amounts of PO always results in the formation of a stable sol without noticeable warming of the reaction mixture. One should be aware of the reactivity and moderate toxicity of PO and take appropriate safety precautions. Reactions involving metal salts and PO can be quite exothermic and often lead to a rapid warming up of the reaction mixture. After 15 min of PO addition, 20 mL of ethanol, followed by surfactant solution (CTAB 1 gm + 30 mL DW) were added up on constant stirring. The purpose of using CTAB is to control the nanoparticle size and shape by selectively or more strongly binding to the emerging crystal facets. CTAB is a quaternary ammonium surfactant play a key role in nanoparticle synthesis by adsorbing to the surface of the forming nanoparticle and lowering its surface energy, thereby preventing their aggregation.

In part-ii, Cu-doped zinc oxide was prepared by replacing an amount of zinc nitrate corresponding to 0−10% molar fraction (doping level) of copper. The total quantity of Zn and Cu nitrates used always added to 0.6 M. Otherwise, the procedure was identical to the one used in part-i. Finally, in part-iii, the addition of GO in the best optimized Cu-doped ZnO sample was carried out. The purpose of loading GO is to enhance the surface area and electrical conductivity, needed for the better gas sensing property. Graphene is a promising gas-sensing material owing to its superb electronic mobility and high specific surface area. Its conductive channels promotes a sort of catalytic behavior (spill-over) required for the improved gas performance. Therefore the best optimized sample was treated to GO loading for further enhancement in the gas-sensing properties.

GO (1 mg) was ultrasonicated in 10 mL DW and added to the slot of the precursor solvent, which was made in 20 mL of DW so as to maintain the concentration equilibrium of 30 mL DW as per earlier parts (i & ii). Rest of the procedures were as described in the aforementioned parts (i & ii).

All the obtained sols were treated to microwave hydrothermal process. To do so, the respective sols were transferred to microwave free reaction vessel autoclaves with Teflon liner, and placed inside the usual domestic microwave unit (IFB-25SC4, with Microwave i/o power as 1400/900 W). The main characteristic microwave parameters are power and time, which needs to be adjusted carefully for attaining the desired subcritical region of water for hydrothermal reaction. For such domestic microwave systems, the reaction temperature and pressure in the autoclaves resulting from microwave irradiation are difficult to measure from the microwave power and exposure time alone. Therefore few trial-and-error experiments were performed with the combination of microwave power and the reaction time. The decent combination of them was found to be 40% power with 10 min time, where precipitate was formed under controlled temperature and pressure without any spillage of reaction mixture. The obtained precipitate was washed thoroughly with ample amount of water to get rid of the used surfactant and unreacted moieties if any. The precipitate was dried at 80 °C for 2 h and sintered at 400 °C for 2 h in air [see thermogravimetry−differential thermal analysis (TG−DTA), S1]. Using screen printing technique, the thick films of the respective samples were developed on the alumina substrates, and sintered at 400 °C for 1 h in air to

https://dx.doi.org/10.1021/acsomega.9b04475
ACS Omega 2020, 5, 8587−8595

remove the added binders from the thixotropic paste. The details of thixotropic paste formation and thereby thick film formation are described in the Supporting Information section (S2). The samples were labeled as "Zn"-for pristine ZnO, "ZC1, ZC2, ZC3, ZC4, ZC5"-for Cu doped ZnO (1.25, 2.5, 5, 7.5, 10 mol %, respectively), and GO_ZC2-for GO loaded 2.5 mol % Cu doped ZnO.

■ ASSOCIATED CONTENT

Supporting Information

The Supporting Information is available free of charge at https://pubs.acs.org/doi/10.1021/acsomega.9b04475.

Performance comparison table of the developed CuO/ZnO nanocomposites with state-of-the-art results in the similar field (Table S1); TG−DTA analysis of the CuO/ZnO nanocomposite (Figure S1); details of thixotropic paste formation and thereby thick films (Figure S2); SEM images of the samples at various Cu doping levels (Figure S3); and elemental mapping and EDX spectra of the sample ZC2, respectively (Figures S4, S5) (PDF)

■ AUTHOR INFORMATION

Corresponding Authors

Hyosung Choi − *Department of Chemistry and Research Institute for Convergence of Basic Sciences, Hanyang University, Seoul 04763, Republic of Korea;* orcid.org/0000-0003-4573-9012; Email: hschoi202@gmail.com

Sharad S. Suryavanshi − *School of Physical Sciences, PAH Solapur University, Solapur 413255, Maharashtra, India;* orcid.org/0000-0002-3996-1998; Email: sssuryavanshi@rediffmail.com

Authors

Digambar Y. Nadargi − *School of Physical Sciences, PAH Solapur University, Solapur 413255, Maharashtra, India;* orcid.org/0000-0003-2092-2590

Mohaseen S. Tamboli − *Department of Chemistry and Research Institute for Convergence of Basic Sciences, Hanyang University, Seoul 04763, Republic of Korea*

Santosh S. Patil − *Department of Chemistry, Pohang University of Science and Technology (POSTECH), Pohang 37673, Republic of Korea*

Ramesh B. Dateer − *Centre for Nano and Material Sciences, JAIN (Deemed-to-be-University), Bangalore, Karnataka 562112, India;* orcid.org/0000-0002-1573-5259

Imtiaz S. Mulla − *Former Emeritus Scientist (CSIR), Centre for Materials for Electronics Technology, Pune 411008, India*

Complete contact information is available at: https://pubs.acs.org/10.1021/acsomega.9b04475

Notes

The authors declare no competing financial interest.

■ ACKNOWLEDGMENTS

The authors greatly acknowledge the CSIR, India, for financial support of this work (03(1389)/16/EMR-II). Dr. Nadargi acknowledges the CSIR, India, for awarding Research Associate under the same scheme. Dr. Dateer acknowledges the SERB-DST, Government of India, for the financial support through the research grant file no. SB/S2/RJN-042/2017 and ECR/2017/002207. This work was supported by the National Research Foundation of Korea (NRF-2019K1A3A1A39103027).

■ REFERENCES

(1) Zhang, J.; Qin, Z.; Zeng, D.; Xie, C. Metal-oxide-semiconductor based gas sensors: screening, preparation, and integration. *Phys. Chem. Chem. Phys.* **2017**, *19*, 6313−6329.

(2) Hahn, S. H.; Bârsan, N.; Weimar, U.; Ejakov, S. G.; Visser, J. H.; Soltis, R. E. CO Sensing with SnO2 Thick Film Sensors: Role of Oxygen and Water Vapour. *Thin Solid Films* **2003**, *436*, 17−24.

(3) He, X.; Li, J.; Gao, X.; Wang, L. NO_2 Sensing Characteristics of WO_3 Thin Film Microgas Sensor. *Sens. Actuators, B* **2003**, *93*, 463−467.

(4) Korotcenkov, G.; Brinzari, V.; Golovanov, V.; Blinov, Y. Kinetics of gas Response to Reducing Gases of SnO_2 Films, Deposited by Spray Pyrolysis. *Sens. Actuators, B* **2004**, *98*, 41−45.

(5) Bai, S.; Li, D.; Han, D.; Luo, R.; Chen, A.; Chung, C. L. Preparation, Characterization of WO_3−SnO_2 Nanocomposites and their Sensing Properties for NO_2. *Sens. Actuators, B* **2010**, *150*, 749−755.

(6) Mehta, S. S.; Nadargi, D. Y.; Tamboli, M. S.; Chaudhary, L. S.; Patil, P. S.; Mulla, I. S.; Suryavanshi, S. S. Ru-Loaded Mesoporous WO_3 Microflowers for Dual Applications: Enhanced H_2S Sensing and Sunlight-driven Photocatalysis. *Dalton Trans.* **2018**, *47*, 16840−16845.

(7) Ju, D.-X.; Xu, H.-Y.; Qiu, Z.-W.; Zhang, Z.-C.; Xu, Q.; Zhang, J.; Wang, J.-Q.; Cao, B.-Q. Near Room Temperature, Fast-Response, and Highly Sensitive Triethylamine Sensor Assembled with Au-Loaded ZnO/SnO_2 Core-Shell Nanorods on Flat Alumina Substrates. *ACS Appl. Mater. Interfaces* **2015**, *7*, 19163−19171.

(8) de Melo, C.; Jullien, M.; Battie, Y.; Naciri, A.; Ghanbaja, J.; Montaigne, F.; Pierson, J.; Rigoni, F.; Almqvist, N.; Vomiero, A.; Migot, S.; Mücklich, F.; Horwat, D. Semi-Transparent p-Cu_2O/n-ZnO Nanoscale-Film Heterojunctions for Photodetection and Photovoltaic Applications. *ACS Appl. Nano Mater.* **2019**, *2*, 4358−4366.

(9) Liu, X.; Du, B.; Sun, Y.; Yu, M.; Yin, Y.; Tang, W.; Chen, C.; Sun, L.; Yang, B.; Cao, W.; Ashfold, M. N. R. Sensitive Room Temperature Photoluminescence-Based Sensing of H_2S with Novel CuO−ZnO Nanorods. *ACS Appl. Mater. Interfaces* **2016**, *8*, 16379−16385.

(10) Zhang, X.; He, X.; Kang, Z.; Cui, M.; Yang, D.-P.; Luque, R. Waste Eggshell-Derived Dual-Functional CuO/ZnO/Eggshell Nanocomposites: (Photo)catalytic Reduction and Bacterial Inactivation. *ACS Sustainable Chem. Eng.* **2019**, *7*, 15762−15771.

(11) Marín, L.; Gao, Y.; Vallet, M.; Abdallah, I.; Warot-Fonrose, B.; Tenailleau, C.; Lucero, A. T.; Kim, J.; Esteve, A.; Chabal, Y. J.; Rossi, C. Performance Enhancement via Incorporation of ZnO Nanolayers in Energetic Al/CuO Multilayers. *Langmuir* **2017**, *33*, 11086−11093.

(12) Kargar, A.; Jing, Y.; Kim, S. J.; Riley, C. T.; Pan, X.; Wang, D. ZnO/CuO Heterojunction Branched Nanowires for Photoelectrochemical Hydrogen Generation. *ACS Nano* **2013**, *7*, 11112−11120.

(13) Wang, C.; Zhu, J.; Liang, S.; Bi, H.; Han, Q.; Liu, X.; Wang, X. Reduced Graphene Oxide Decorated with CuO−ZnO Heterojunctions: Towards High Selective Gas-sensing Property to Acetone. *J. Mater. Chem. A* **2014**, *2*, 18635−18643.

(14) Xu, K.; Wu, J.; Tan, C. F.; Ho, G. W.; Wei, A.; Hong, M. Ag−CuO−ZnO Metal−Semiconductor Multiconcentric Nanotubes for Achieving Superior and Perdurable Photodegradation. *Nanoscale* **2017**, *9*, 11574−11583.

(15) Chen, Y.; Shen, Z.; Jia, Q.; Zhao, J.; Zhao, Z.; Ji, H. A CuO−ZnO Nanostructured p−n Junction Sensor for Enhanced N-butanol Detection. *RSC Adv.* **2016**, *6*, 2504−2511.

(16) Koebel, M. M.; Nadargi, D. Y.; Jimenez-Cadena, G.; Romanyuk, Y. E. Transparent, Conducting ATO Thin Films by Epoxide-Initiated Sol-Gel Chemistry: A Highly Versatile Route to Mixed-Metal Oxide Films. *ACS Appl. Mater. Interfaces* **2012**, *4*, 2464−2473.

(17) Gash, A. E.; Satcher, J. H.; Simpson, R. L. Strong Akaganeite Aerogel Monoliths Using Epoxides: Synthesis and Characterization. *Chem. Mater.* **2003**, *15*, 3268−3275.
(18) Rana, A. u. H. S.; Kang, M.; Kim, H. Microwave-assisted Facile and Ultrafast Growth of ZnO Nanostructures and Proposition of Alternative Microwave-assisted Methods to Address Growth Stoppage. *Sci. Rep.* **2016**, *6*, 24870.
(19) Schmidt, R.; Gonjal, J.; Moran, E. Microwaves Microwave-Assisted Hydrothermal Synthesis of Nanoparticles. *CRC Concise Encyclopedia of Nanotechnology*; CRC Press Taylor & Francis, 2015. ISBN: 978-1-4665-8034-3.
(20) Zhu, L.; Li, H.; Liu, Z.; Xia, P.; Xie, Y.; Xiong, D. Synthesis of the 0D/3D CuO/ZnO Heterojunction with Enhanced Photocatalytic Activity. *J. Phys. Chem. C* **2018**, *122*, 9531−9539.
(21) Nadargi, D. Y.; Dateer, R. B.; Tamboli, M. S.; Mulla, I. S.; Suryavanshi, S. S. A Greener Approach Towards the Development of Graphene−Ag Loaded ZnO Nanocomposites for Acetone Sensing Applications. *RSC Adv.* **2019**, *9*, 33602.
(22) Nadargi, D. Y.; Tamboli, M. S.; Patil, S. S.; Mulla, I. S.; Suryavanshi, S. S. Development of Ag/ZnO Nanorods and Nanoplates at Low Hydrothermal Temperature and Time for Acetone Sensing Application: an insight into Spillover Mechanism. *SN Appl. Sci.* **2019**, *1*, 1564.
(23) Mirzaei, A.; Kim, S. S.; Kim, H. W. Resistance-based H2S Gas Sensors using Metal Oxide Nanostructures: A Review of Recent Advances. *J. Hazard. Mater.* **2018**, *357*, 314−331.
(24) Zhang, J.; Qin, Z.; Zeng, D.; Xie, C. Metal-Oxide-Semiconductor based Gas sensors: Screening, Preparation, and Integration. *Phys. Chem. Chem. Phys.* **2017**, *19*, 6313−6329.
(25) Xue, D.; Zhou, R.; Lin, X.; Duan, X.; Li, Q.; Wang, T. A Highly Selective and Sensitive H_2S Sensor at Low Temperatures based on Cr-doped α-Fe_2O_3 nanoparticles. *RSC Adv.* **2019**, *9*, 4150−4156.
(26) Garner, W. E.; Gray, T. J.; Stone, F. S.; Savage, S. D.; Tiley, P. F. Reactions on the surface of copper oxide. *Discuss. Faraday Soc.* **1950**, *8*, 246.
(27) Shao, F.; Hoffmann, M. W. G.; Prades, J. D.; Zamani, R.; Arbiol, J.; Morante, J. R.; Varechkina, E.; Rumyantseva, M.; Gaskov, A.; Giebelhaus, I.; Fischer, T.; Mathur, S.; Hernández-Ramírez, F. Heterostructured p-CuO (nanoparticle)/n-SnO_2 (nanowire) devices for selective H_2S detection. *Sens. Actuators, B* **2013**, *181*, 130−135.
(28) Choi, S.-W.; Katoch, A.; Zhang, J.; Kim, S. S. Electrospun nanofibers of CuO-SnO_2 nanocomposite as semiconductor gas sensors for H_2S detection. *Sens. Actuators, B* **2013**, *176*, 585−591.
(29) Lei, H.; Qin, P.; Ke, W.; Guo, Y.; Dai, X.; Chen, Z.; Wang, H.; Li, B.; Zheng, Q.; Fang, G. Performance enhancement of polymer solar cells with high work function CuS modified ITO as anodes. *Org. Electron.* **2015**, *22*, 173−179.
(30) Song, Z.; Lei, H.; Li, B.; Wang, H.; Wen, J.; Li, S.; Fang, G. Enhanced field emission from in situ synthesized 2D copper sulfide nanoflakes at low temperature by using a novel controllable solvothermal preferred edge growth route. *Phys. Chem. Chem. Phys.* **2015**, *17*, 11790−11795.
(31) Basu, M.; Nazir, R.; Fageria, P.; Pande, S. Construction of CuS/Au heterostructure through a simple photoreduction route for enhanced electrochemical hydrogen evolution and photocatalysis. *Sci. Rep.* **2016**, *6*, 34738.
(32) Lei, H.; Fang, G.; Cheng, F.; Ke, W.; Qin, P.; Song, Z.; Zheng, Q.; Fan, X.; Huang, H.; Zhao, X. Enhanced efficiency in organic solar cells via in situ fabricated p-type copper sulfide as the hole transporting layer. *Sol. Energy Mater. Sol. Cells* **2014**, *128*, 77−84.
(33) Park, S.; Kim, S.; Kheel, H.; Hyun, S. K.; Jin, C.; Lee, C. Enhanced H_2S gas sensing performance of networked CuO-ZnO composite nanoparticle sensor. *Mater. Res. Bull.* **2016**, *82*, 130−135.
(34) Wang, L.; Kang, Y.; Wang, Y.; Zhu, B.; Zhang, S.; Huang, W.; Wang, S. CuO nanoparticle decorated ZnO nanorod sensor for low-temperature H_2S detection. *Mater. Sci. Eng., C* **2012**, *32*, 2079−2085.
(35) Kim, S.-J.; Na, C. W.; Hwang, I.-S.; Lee, J.-H. One-pot hydrothermal synthesis of CuO-ZnO composite hollow spheres for selective H_2S detection. *Sens. Actuators, B* **2012**, *168*, 83−89.
(36) Xu, Z.; Duan, G.; Li, Y.; Liu, G.; Zhang, H.; Dai, Z.; Cai, W. CuO-ZnO Micro/Nanoporous Array-Film-Based Chemosensors: New Sensing Properties to H_2S. *Chem.—Eur. J.* **2014**, *20*, 6040−6046.
(37) Katoch, A.; Choi, S.-W.; Kim, J.-H.; Lee, J. H.; Lee, J.-S.; Kim, S. S. Importance of the nanograin size on the H_2S-sensing properties of ZnO-CuO composite nanofibers. *Sens. Actuators, B* **2015**, *214*, 111−116.
(38) Datta, N.; Ramgir, N.; Kaur, M.; Ganapathi, S. K.; Debnath, A. K.; Aswal, D. K.; Gupta, S. K. Elective H_2S sensing characteristics of hydrothermally grown ZnO-nanowires network tailored by ultrathin CuO layers. *Sens. Actuators, B* **2012**, *166−167*, 394−401.
(39) Huang, J.; Dai, Y.; Gu, C.; Sun, Y.; Liu, J. Preparation of porous flower-like CuO/ZnO nanostructures and analysis of their gas-sensing property. *J. Alloys Compd.* **2013**, *575*, 115−122.

https://dx.doi.org/10.1021/acsomega.9b04475
ACS Omega 2020, 5, 8587−8595